J. Fluid Mech. (1983), *vol.* 129, *pp.* 409–426
Printed in Great Britain

A viscous vortex pair in ground effect

By A. J. PEACE AND N. RILEY
School of Mathematics and Physics, University of East Anglia, Norwich NR4 7TJ, U.K.

(Received 16 August 1982)

We calculate the flow induced by a vortex pair in a viscous fluid, which is otherwise at rest, in the presence of a plane boundary. This may be either a no-slip or a stress-free boundary. The phenomenon of rebound of the vortices from the boundary occurs for either type of boundary, and an explanation for this is offered in terms of viscous effects.

1. Introduction

In this paper we are concerned with the unsteady fluid motion which is induced when a vortex pair moves in an incompressible viscous fluid towards a plane boundary. The vortex pair at the initial instant is represented by two inviscid line vortices and the line which joins them is parallel to the boundary surface, which may be either a rigid boundary at which the no-slip condition must be satisfied or a free surface corresponding to zero shear stress.

In § 2 we first of all construct an asymptotic solution to describe the early stages of the motion. For the case of a no-slip boundary this is dominated by the rapid diffusion of vorticity from the boundary, with its attendant displacement effect, and the rapid diffusion of vorticity from the neighbourhood of the line vortex; for the case of a free surface only the latter is involved. The solution is carried beyond the initial stages via a direct numerical integration of the unsteady Navier–Stokes equations. The method which is used is also described in § 2 and is based upon the split-operator idea in which an iteration takes place between the equations for the vorticity and stream function. The former is parabolic and an alternating-direction implicit method is used for its solution, whilst the latter is elliptic and solved by successive-point over-relaxation.

The results of our numerical calculations are described in § 3 for values of a suitably defined Reynolds number up to 150. The principal features are the decay of the vorticity, and the trajectory of the vortex centre. Free-flight observations (Dee & Nicholas 1968; Tombach, Crow & Bate 1975) indicate that the trailing vortices behind an aircraft move at first toward the ground, as on an inviscid trajectory, and then away from it. Laboratory experiments by Harvey & Perry (1971), Barker & Crow (1977) and Wickens (1980) confirm this behaviour, with the experiments of Barker & Crow, carried out in water, demonstrating that the phenomenon also occurs at a free surface where the shear stress vanishes. For a rigid boundary a satisfactory explanation for the vortex rebound has been given by Harvey & Perry based upon flow separation. However, for the case of a free surface that explanation is not valid, and Barker & Crow suggest an inviscid argument based upon a finite vortex-core size; this conjecture is found by Saffman (1979) to be unacceptable. It is our view that the rebound phenomenon owes its origins to viscous effects regardless of whether or not the boundary is one of no-slip or zero shear. Similar numerical calculations to ours have also been carried out by Grove (1981) which also demonstrate the rebound

effect. However, a direct comparison between the two is not possible owing to differences in the initial conditions.

2. Governing equations and solution procedure

As we have indicated above, we consider the situation in which the flow due to an initially inviscid vortex pair in the presence of the plane boundary $y' = 0$ develops with time under the action of viscosity. With reference to Cartesian coordinates (x', y') the vortices, of strength $\pm\Gamma$, are situated at $(\pm d, h)$. If the fluid has density ρ and kinematic viscosity ν we choose d, d^2/Γ, Γ/d, $\rho\Gamma^2/d^2$ as typical length, time, velocity and pressure respectively, so that the dimensionless governing equations, for our two-dimensional flow, may be written as

$$\frac{\partial \mathbf{v}}{\partial t} + (\mathbf{v} \cdot \nabla)\,\mathbf{v} = -\nabla p + \frac{1}{R}\nabla^2 \mathbf{v}, \tag{2.1}$$

$$\nabla \cdot \mathbf{v} = 0, \tag{2.2}$$

where $R = \Gamma/\nu$ is the Reynolds number of the flow, p is the pressure and $\mathbf{v} = (u, v)$ the velocity vector. In much of what follows it proves convenient to work not with the primitive variables of (2.1) and (2.2) but with the stream function and vorticity. Thus we introduce the stream function ψ such that

$$u = \frac{\partial \psi}{\partial y}, \quad v = -\frac{\partial \psi}{\partial x}, \tag{2.3}$$

and then with the vorticity $\boldsymbol{\zeta} = (0, 0, \zeta)$ we have, upon eliminating p from (2.1), and using (2.2),

$$\frac{\partial \zeta}{\partial t} + \nabla \cdot (\mathbf{v}\zeta) = \frac{1}{R}\nabla^2 \zeta, \tag{2.4}$$

with

$$\nabla^2 \psi = -\zeta. \tag{2.5}$$

The boundary conditions required are as follows. At $t = 0$ we have the flow due to an inviscid vortex pair throughout the flow region. For $t > 0$ we have $\psi = \zeta = 0$ on $x = 0$, $0 < y < \infty$, with $\psi = 0$ on $y = 0$, $x \geqslant 0$. In addition, for a solid boundary we require the no-slip condition to be satisfied at $y = 0$, which we interpret as a condition on ζ in § 2.2; by contrast, for a stress-free boundary at $y = 0$, which models a clean undeformed free surface, we have simply $\zeta = 0$.

2.1. *The initial flow development*

At the initial instant $t = 0$ the flow is that due to isolated line vortices at $(1, \pm h/d)$, together with a vortex sheet on $y = 0$. The effect of viscosity is to diffuse vorticity rapidly from these singular regions, and we now construct solutions which describe this process. On account of symmetry we need only consider the solution in $x, y \geqslant 0$. It proves convenient to develop the solution separately in the viscous wall region, the viscous neighbourhood of the line vortex, and an 'outer' region within which the solution is essentially an inviscid one. The stream function identified within each of these regions is identified by a superscript 'w', 'v' and 'o' respectively. In each region the stream function is conveniently represented, for small values of t, in the form

$$\phi = \phi_0(x, y, t;\, R) + \left(\frac{t}{R}\right)^{\frac{1}{2}} \phi_1(x, y, t;\, R) + \left(\frac{t}{R}\right) \phi_2(x, y, t;\, R) + O\left\{\left(\frac{t}{R}\right)^{\frac{3}{2}}\right\}, \tag{2.6}$$

and asymptotic matching between the different regions is carried out. It should be emphasized that the coefficients in (2.6) may contain terms $O(R^n)$, so that in the limit $R \to \infty$ the expansion (2.6) becomes that which is familiar in classical boundary-layer theory.

We consider first the interaction between the wall layer for the case of a no-slip boundary and the outer inviscid region, and finally consider the solution in the neighbourhood of the line vortex. This procedure is permissible since, as we shall see, the terms up to and including $O(t/R)$ in the vortex region bring about no modification to the outer inviscid flow.

The leading term in the outer solution, represented in the form (2.6), is given simply as

$$\psi_0^{(0)} = -\frac{1}{4\pi} \log \frac{\{(x-x_0)^2+(y-y_0)^2\}\{(x+x_0)^2+(y+y_0)^2\}}{\{(x+x_0)^2+(y-y_0)^2\}\{(x-x_0)^2+(y+y_0)^2\}}, \tag{2.7}$$

which corresponds to a line vortex at $x = x_0(t)$, $y = y_0(t)$, where

$$\frac{dx_0}{dt} = \frac{x_0^2}{4\pi y_0(x_0^2+y_0^2)}, \quad \frac{dy_0}{dt} = -\frac{y_0^2}{4\pi x_0(x_0^2+y_0^2)}, \tag{2.8}$$

with $x_0(0) = 1$, $y_0(0) = h/d$. The solution (2.7), with (2.3), implies a velocity of slip at $y = 0$ given by

$$U_0(x,t) = \frac{4}{\pi} \frac{x_0 y_0 x}{\{(x-x_0)^2+y_0^2\}\{(x+x_0)^2+y_0^2\}}. \tag{2.9}$$

For the wall layer we write $\psi = 2(t/R)^{\frac{1}{2}}\psi^{(w)}$ and expand $\psi^{(w)}$ as in (2.6). Thus with $\psi_0^{(w)} = U_0 f_0(\eta)$, where $\eta = \frac{1}{2}y(R/t)^{\frac{1}{2}}$, we have from (2.3)–(2.5)

$$\left.\begin{aligned} f_0''' + 2\eta f_0'' &= 0, \\ f_0(0) = f_0'(0) = 0, \quad f_0'(\infty) &= 1, \end{aligned}\right\} \tag{2.10}$$

with

where the condition at $\eta = \infty$ ensures a match with the outer solution, and a prime denotes differentiation with respect to η. The solution for f_0 is the classical solution

$$f_0 = \eta \operatorname{erf} \eta + \frac{1}{\pi^{\frac{1}{2}}} e^{-\eta^2} - \frac{1}{\pi^{\frac{1}{2}}}. \tag{2.11}$$

We can see from (2.11) that $f_0 - \eta \to -\pi^{-\frac{1}{2}}$ as $\eta \to \infty$: this implies that the next term in the outer expansion, of the form (2.6), arises from a source distribution on $y = 0$ of strength $2\pi^{-\frac{1}{2}}\partial U_0/\partial x$ per unit length. Thus with $\nabla^2\psi_1^{(0)} = 0$, from (2.4), (2.5) and with $\psi_1^{(0)} = 0$ on $x = 0$, $\psi_1^{(0)} \to 0$ as $x^2+y^2 \to \infty$, we have

$$\psi_1^{(0)} = \frac{2}{\pi^{\frac{3}{2}}} \int_{-\infty}^{\infty} \left.\frac{\partial U_0}{\partial x}\right|_{x=\xi} \tan^{-1}\frac{y}{x-\xi}\, d\xi, \tag{2.12}$$

which makes a contribution $U_1(t/R)^{\frac{1}{2}}$ to the velocity of slip on $y = 0$, where U_1 is given by

$$U_1(x,t) = \frac{2}{\pi^{\frac{3}{2}}} \int_{-\infty}^{\infty} \left.\frac{\partial U_0}{\partial x}\right|_{x=\xi} \frac{d\xi}{x-\xi}, \tag{2.13}$$

and the Cauchy principal value of the integral in (2.13) is to be understood. Thus for our second term in the expansion for $\psi^{(w)}$ we write $\psi_1^{(w)} = U_1 f_1(\eta)$ so that, again from (2.3)–(2.5) we have

$$\left.\begin{aligned} f_1''' + 2\eta f_1''/2f_1' &= -2, \\ f_1(0) = f_1'(0) = 0, \quad f_1'(\infty) &= 1, \end{aligned}\right\} \tag{2.14}$$

with solution

$$f_1 = \eta + \tfrac{1}{2}\pi^{\frac{1}{2}}\eta^2 \operatorname{erfc}\eta - \tfrac{1}{2}\eta\, e^{-\eta^2} - \tfrac{1}{4}\pi^{\frac{1}{2}} \operatorname{erf}\eta. \tag{2.15}$$

We note that $f_1 - \eta \to -\frac{1}{4}\pi^{\frac{1}{2}}$ as $\eta \to \infty$, which shows that the wall layer contributes a source effect at $O(t/R)$ to the outer solution. Thus since it can be shown that $\psi_2^{(0)}$ is a harmonic function we have

$$\psi_2^{(0)} = \frac{1}{2\pi^{\frac{1}{2}}} \int_{-\infty}^{\infty} \left.\frac{\partial U_1}{\partial x}\right|_{x=\xi} \tan^{-1}\frac{y}{x-\xi}\, d\xi. \tag{2.16}$$

The solution in the outer region is now complete up to and including terms $O(t/R)$. However, (2.16) implies a slip velocity $U_2(t/R)$ at $y = 0$, with

$$U_2(x,t) = \frac{1}{2\pi^{\frac{1}{2}}} \int_{-\infty}^{\infty} \left.\frac{\partial U_1}{\partial x}\right|_{x=\xi} \frac{d\xi}{x-\xi}, \tag{2.17}$$

where again the Cauchy principal value is to be understood. To complete the solution in the wall layer to this order we now write

$$\psi_2^{(w)} = R\left\{U_0 \frac{\partial U_0}{\partial x} f_{20}(\eta) + \frac{\partial U_0}{\partial t} f_{21}(\eta)\right\} + \frac{\partial^2 U_0}{\partial x^2} f_{22}(\eta) + U_2 f_{23}(\eta). \tag{2.18}$$

The first two terms of (2.18), with coefficient R, are recognizable as the terms which arise in the infinite Reynolds number, or boundary-layer, limit in the study of impulsive flows; the last term is required to match the slip velocity (2.17). The remaining term arises from contributions from the right-hand side of (2.4) and because of the necessity to match with the outer solution. In this latter respect we note that the inner expansions of both $\psi_0^{(0)}$ and $\psi_1^{(0)}$ yield contributions with which f_{22} must match. The equations satisfied by f_{2i}, $i = 0, \ldots, 3$, are, using (2.4)–(2.6),

$$\left.\begin{aligned} f_{2i}''' + 2\eta f_{2i}'' - 4f_{2i}' &= F_i, \\ F_0 = 4(f_0'^2 - f_0 f_0'' - 1), \quad F_1 &= 4(f_0' - 1), \\ F_2 = 16\int_0^{\eta} f_0\, d\eta - 8\eta f_0 - 8f_0', \quad F_3 &= -4, \end{aligned}\right\} \tag{2.19}$$

where

together with boundary conditions

$$\left.\begin{aligned} f_{2i}(0) = f_{2i}'(0) &= 0 \quad (i = 0, \ldots, 3), \\ f_{20}'(\infty) = f_{21}'(\infty) &= 0, \\ f_{22}' \sim -2\eta^2 + \frac{4}{\pi^{\frac{1}{2}}}\eta, \quad f_{23}' &\sim 1 \quad \text{as} \quad \eta \to \infty. \end{aligned}\right\} \tag{2.20}$$

The asymptotic forms for f_{22}' and f_{23}' are as dictated by the matching requirement. For f_{20} we have, as given by Blasius (1908),

$$\begin{aligned} f_{20}' = &-\frac{3}{\pi^{\frac{1}{2}}}\eta\, e^{-\eta^2} \operatorname{erfc}\eta + \tfrac{1}{2}(2\eta^2 - 1)\operatorname{erfc}^2\eta + \frac{2}{\pi} e^{-2\eta^2} + \frac{1}{\pi^{\frac{1}{2}}}\eta\, e^{-\eta^2} \\ &+ 2\operatorname{erfc}\eta - \frac{4}{3\pi} e^{-\eta^2} + \left(\frac{3}{\pi^{\frac{1}{2}}} + \frac{4}{3\pi^{\frac{3}{2}}}\right)\{\eta\, e^{-\eta^2} - \tfrac{1}{2}\pi^{\frac{1}{2}}(2\eta^2 + 1)\operatorname{erfc}\eta\}, \end{aligned}$$

from which f_{20} is obtained by quadrature, and the solutions of (2.19) for $i = 1, 2, 3$ are given by

$$f_{21} = \frac{1}{3\pi^{\frac{1}{2}}}(1-e^{-\eta^2}) - \tfrac{2}{3}\eta^3 \operatorname{erfc}\eta + \frac{2}{3\pi^{\frac{1}{2}}}\eta^2 e^{-\eta^2},$$

$$f_{22} = \frac{1}{3\pi^{\frac{1}{2}}}(e^{-\eta^2}-1) - \tfrac{2}{3}\eta^3 \operatorname{erf}\eta - \frac{2}{3\pi^{\frac{1}{2}}}\eta^2 e^{-\eta^2} + \frac{2}{\pi^{\frac{1}{2}}}\eta^2,$$

$$f_{23} = \eta \operatorname{erf}\eta - \tfrac{2}{3}\eta^3 \operatorname{erfc}\eta + \frac{2}{3\pi^{\frac{1}{2}}}(\eta^2 e^{-\eta^2} + e^{-\eta^2} - 1).$$

The solution for $\psi^{(w)}$ is now complete to $O(t/R)$.

We consider next the solution in the neighbourhood of the isolated vortices under the influence of the outer solution $\psi^{(o)}$. As before, we need only consider the flow in the first quadrant, and it will be necessary for us to ensure, as asserted above, that the outer flow we have calculated is not modified up to $O(t/R)$. It proves convenient at this stage to work with coordinates with origin at the vortex centre (X_v, Y_v), which is defined as the position at which the vorticity has a local maximum. Quantities associated with these coordinates are denoted by an overbar and we note that (2.3)–(2.5) otherwise remain unchanged. It also proves convenient to write

$$\psi^{(o)} = \tilde{\psi}^{(o)} - \frac{1}{2\pi}\log\bar{r}, \tag{2.21}$$

where $\bar{r}^2 = \bar{x}^2 + \bar{y}^2$, and then to write

$$\bar{\psi}^{(o)} = \tilde{\psi}^{(o)} - \frac{1}{2\pi}\log\bar{r} - \dot{X}_v\bar{y} + \dot{Y}_v\bar{x} - \tilde{\psi}^{(o)}|_0, \tag{2.22}$$

where a dot denotes differentiation with respect to t and the subscript 0 denotes $\bar{x} = \bar{y} = 0$. An expansion of the form (2.6) is already available for $\tilde{\psi}^{(o)}$ from our discussion of the outer solution, and we now assume that $(\dot{X}_v, \dot{Y}_v)$ can be expanded in a similar manner. We also anticipate that an appropriate viscous coordinate is $\bar{\eta} = \frac{1}{2}\bar{r}(R/t)^{\frac{1}{2}}$. We next write the outer solution (2.22) in terms of the inner variables $(\bar{\eta}, \theta)$, where θ is a conventional angular coordinate measured from $\bar{y} = 0$, to give

$$-\frac{1}{2\pi}\log\left[4\left(\frac{t}{R}\right)\right] - \frac{1}{2\pi}\log\bar{\eta} + 2\left(\frac{t}{R}\right)^{\frac{1}{2}}\bar{\eta}(\bar{U}_0\sin\theta - \bar{V}_0\cos\theta)$$
$$+2\left(\frac{t}{R}\right)\left\{\bar{\eta}^2\left(\cos 2\theta\frac{\partial^2\tilde{\psi}_0^{(o)}}{\partial\bar{x}^2}\bigg|_0 + \sin 2\theta\frac{\partial^2\tilde{\psi}_0^{(o)}}{\partial\bar{x}\,\partial\bar{y}}\bigg|_0\right) + \bar{\eta}(\bar{U}_1\sin\theta - \bar{V}_1\cos\theta)\right\}, \tag{2.23}$$

where we have written

$$\bar{U}_i = \frac{\partial\tilde{\psi}_i^{(o)}}{\partial\bar{y}}\bigg|_0 - \dot{X}_i, \quad \bar{V}_i = -\frac{\partial\tilde{\psi}_i^{(o)}}{\partial\bar{x}}\bigg|_0 - \dot{Y}_i, \quad (i = 0, 1), \tag{2.24}$$

as the components of velocity at the vortex centre. The expression (2.23) now provides an outer expansion for the inner-vortex solution.

In addition to working with an expansion of the form (2.6) for $\bar{\psi}^{(v)}$ in the vortex region it is convenient to introduce the vorticity. Thus with $\bar{\zeta} = \frac{1}{4}(R/t)\bar{\zeta}^{(v)}$ and an expansion of the form (2.6) for $\bar{\zeta}^{(v)}$ assumed, we note, from (2.23), that we may expect the leading term to be independent of θ. Thus we have, from (2.4),

$$\frac{d^2\bar{\zeta}_0^{(v)}}{d\bar{\eta}^2} + \left(\frac{1}{\bar{\eta}} + 2\bar{\eta}\right)\frac{d\bar{\zeta}_0^{(v)}}{d\bar{\eta}} + 4\bar{\zeta}_0^{(v)} = 0,$$

with solution, which matches with (2.23) as $\bar{\eta} \to \infty$,

$$\bar{\zeta}_0^{(\mathrm{v})} = \frac{1}{\pi} \exp(-\bar{\eta}^2), \tag{2.25}$$

as for example in Lamb (1932).

For the next terms in our expansions for $\bar{\psi}^{(\mathrm{v})}$ and $\bar{\zeta}^{(\mathrm{v})}$, let us write

$$\left.\begin{aligned} \bar{\psi}_1^{(\mathrm{v})} &= \Psi_{1\mathrm{s}}(\bar{\eta}) \sin n\theta - \Psi_{1\mathrm{c}}(\bar{\eta}) \cos n\theta, \\ \bar{\zeta}_1^{(\mathrm{v})} &= Z_{1\mathrm{s}}(\bar{\eta}) \sin n\theta - Z_{1\mathrm{c}}(\bar{\eta}) \cos n\theta, \end{aligned}\right\} \tag{2.26}$$

where the unknown functions of $\bar{\eta}$ satisfy

$$\left.\begin{aligned} Z_{1\mathrm{s}}'' + \left(\frac{1}{\bar{\eta}} + 2\bar{\eta}\right) Z_{1\mathrm{s}}' - \left(\frac{n^2}{\bar{\eta}^2} - 2\right) Z_{1\mathrm{s}} &= \frac{Rn}{\bar{\eta}} (\Psi_{1\mathrm{c}}\, \bar{\zeta}_0^{(\mathrm{v})\prime} - Z_{1\mathrm{c}}\, \bar{\psi}_0^{(\mathrm{v})\prime}), \\ Z_{1\mathrm{c}}'' + \left(\frac{1}{\bar{\eta}} + 2\bar{\eta}\right) Z_{1\mathrm{c}}' - \left(\frac{n^2}{\bar{\eta}^2} - 2\right) Z_{1\mathrm{c}} &= \frac{Rn}{\bar{\eta}} \left(Z_{1\mathrm{s}}\, \bar{\psi}_0^{(\mathrm{v})\prime} - \Psi_{1\mathrm{s}}\, \bar{\zeta}_0^{(\mathrm{v})\prime}\right), \\ \Psi_{1\mathrm{s}}'' + \frac{1}{\bar{\eta}} \Psi_{1\mathrm{s}}' - \frac{n^2}{\bar{\eta}^2} \Psi_{1\mathrm{s}} = -Z_{1\mathrm{s}}, \quad \Psi_{1\mathrm{c}}'' + \frac{1}{\bar{\eta}} \Psi_{1\mathrm{c}}' - \frac{n^2}{\bar{\eta}^2} \Psi_{1\mathrm{c}} &= -Z_{1\mathrm{c}}, \end{aligned}\right\} \tag{2.27}$$

and a prime now denotes differentiation with respect to $\bar{\eta}$. For $\bar{\eta} \ll 1$ it can be shown, if $\bar{\psi}_1^{(\mathrm{v})}$, $\bar{\zeta}_1^{(\mathrm{v})}$ are to remain finite as $\bar{\eta} \to 0$, that all four unknowns behave like $a_i\, \bar{\eta}^n$, where a_i, $i = 1, \ldots, 4$, are constants to be determined. Now it is clear from (2.23) that the case $n = 1$ is of interest to us at this stage, and since $\bar{\zeta}_1^{(\mathrm{v})\prime}$ is required to vanish at $\bar{\eta} = 0$, two of the constants a_i vanish immediately. As a consequence the homogeneous system (2.27) admits only a trivial solution and we conclude that $\bar{U}_0 = \bar{V}_0 = 0$, which in turn, from (2.24), means that X_0, Y_0 may be identified with x_0, y_0 in (2.8), as expected. The final terms which we consider in our expansions for $\bar{\psi}^{(\mathrm{v})}$ and $\bar{\zeta}^{(\mathrm{v})}$, namely $\bar{\psi}_2^{(\mathrm{v})}$, $\bar{\zeta}_2^{(\mathrm{v})}$, may also be split in the manner (2.26), in order to accommodate the matching condition (2.23) where both the cases $n = 1$, 2 are now required. The case $n = 1$ leads, by arguments set out above, immediately to $U_1 = V_1 = 0$ so that X_1, Y_1 are determined from (2.24). For $n = 2$ (2.27), appropriate since $\bar{\psi}_1^{(\mathrm{v})} = \bar{\zeta}_1^{(\mathrm{v})} \equiv 0$, must be solved numerically for $\Psi_{2\mathrm{s,c}}$ and $Z_{2\mathrm{s,c}}$ subject to the matching condition (2.23), and the requirement that algebraic decay at infinity in the vorticity be suppressed. Athough (2.27) are independent of t, that variable does apper parametrically in the solution through (2.23), noting the dependence of $\tilde{\psi}_0^{(\mathrm{o})}$ upon t. The results for $X_{0,1}$ and $Y_{0,1}$ show that, to this order, the vortex centre moves with a velocity determined from the outer inviseid flow. We also see that the asymptotic form for $\bar{\psi}_2^{(\mathrm{v})}$ contains terms as $\bar{\eta} \to \infty$, in addition to those required to match with (2.23), which are $O(\bar{\eta}^{-2} \sin 2\theta, \bar{\eta}^{-2} \cos 2\theta)$. These terms will require a modification to the outer inviscid flow at $O\{(t/R)^2\}$, which, as we have previously asserted, does not affect those terms already obtained in the outer region.

The treatment outlined above is for the initial flow development over a no-slip surface. For the stress-free case the situation is somewhat simpler owing to the absence of the wall layer with its attendant displacement effect.

2.2. *Numerical procedure*

Our aim is to solve (2.4) and (2.5) in the first quadrant $x, y \geqslant 0$ by a finite-difference approach, subject to the spatial boundary conditions stated at the beginning of this section, for $t > t_{\mathrm{I}}$, where the solution at t_{I} is obtained from the small-time solution

developed above. Note that (2.4) is written in conservation form, the importance of which is discussed, for example, in Roache (1972).

The first difficulty we anticipate is that of the application of boundary conditions at infinity. One obvious method is to apply these conditions, as they stand, on a finite outer boundary. However, Bayliss, Gunzberger & Turkel (1982) have shown that large errors can be introduced into the solution by this approximation. We therefore introduce a transformation of the coordinates (x, y) onto a new set of coordinates (X, Y), where

$$\left.\begin{aligned} X &= a(1-e^{-bx}), \\ Y &= a(1-e^{-by}), \end{aligned}\right\} \tag{2.28}$$

where a, b are constants to be chosen. Hence the infinite region $0 \leqslant x < \infty, 0 \leqslant y < \infty$ is mapped onto the finite region $0 \leqslant X \leqslant a, 0 \leqslant Y \leqslant a$. This transformation will also enable us, when a finite-difference mesh is set up, to concentrate grid points in the regions where the gradients are initially large, namely in the vortex region and near the wall. Using (2.28), the governing equations (2.4) and (2.5) now become

$$\frac{\partial \zeta}{\partial t} + b^2(a-X)(a-Y)\left[\frac{\partial}{\partial X}\left(\zeta\frac{\partial \psi}{\partial Y}\right) - \frac{\partial}{\partial Y}\left(\zeta\frac{\partial \psi}{\partial X}\right)\right] = \frac{1}{R}\bar{\nabla}^2\zeta, \tag{2.29}$$

and

$$\bar{\nabla}^2\psi = -\zeta, \tag{2.30}$$

where

$$\bar{\nabla}^2 = b^2\left[(a-X)^2\frac{\partial^2}{\partial X^2} - (a-X)\frac{\partial}{\partial X} + (a-Y)^2\frac{\partial^2}{\partial Y^2} - (a-Y)\frac{\partial}{\partial Y}\right].$$

The spatial boundary conditions now become $\psi = \zeta = 0$ on $X = 0$ and $X = a$, $0 \leqslant Y \leqslant a$ and $Y = a$, $0 \leqslant X \leqslant a$, with $\psi = 0$ on $Y = 0$, $0 \leqslant X \leqslant a$. A condition for ζ on $Y = 0$ remains to be derived for the case of a no-slip boundary; for the stress-free case we have simply $\zeta = 0$ on $Y = 0$, $0 \leqslant X \leqslant a$.

We now set up a uniform rectangular grid in the finite (X, Y)-plane, of dimensions $M \times N$, so that the grid spacings ΔX and ΔY are defined as

$$\Delta X = \frac{a}{M-1}, \quad \Delta Y = \frac{a}{N-1}. \tag{2.31}$$

We must first set up the initial conditions at time $t = t_1$ on this mesh. This is done by first calculating the vorticity ζ from the initial solution described in § 2.1. From this distribution of ζ the stream function ψ is obtained at the initial time t_1 by a direct numerical integration of (2.30) for ψ in the manner outlined below.

We now solve a finite-difference approximation to (2.29) and (2.30) on the finite-difference mesh so that the values of ψ and ζ at each grid point, namely $\psi_{i,j}$ and $\zeta_{i,j}$, $1 \leqslant i \leqslant M$, $1 \leqslant j \leqslant N$, are determined for $t > t_1$. As (2.29) is parabolic in time we can march the vorticity forward in t, with steps of size Δt, whilst ensuring that the elliptic equation (2.30) and the boundary conditions are satisfied throughout. In setting up finite-difference approximations to (2.29) and (2.30) we use central spatial differences, so that $\partial\psi/\partial X$ and $\partial^2\psi/\partial X^2$ are approximated at the grid point (i,j) by

$$\frac{\delta\psi_{i,j}}{\delta X} = \frac{\psi_{i+1,j} - \psi_{i-1,j}}{2\Delta X},$$

$$\frac{\delta^2\psi_{i,j}}{\delta X^2} = \frac{\psi_{i+1,j} - 2\psi_{i,j} + \psi_{i-1,j}}{\Delta X^2}$$

respectively, and similarly for derivatives with respect to Y; similar expressions approximate the spatial derivatives of ζ.

We solve the finite-difference approximation to (2.29) by using an alternating-direction implicit (ADI) method. Let the solution for $\zeta_{i,j}$ at time t be $\zeta^k_{i,j}$; we then wish to obtain the solution at the interior grid points at time $t+\Delta t$, $\zeta^{k+1}_{i,j}$, $2 \leqslant i \leqslant M-1$, $2 \leqslant j \leqslant N-1$: we assume, at this juncture, that ψ and all boundary values are known at both t and $t+\Delta t$. The ADI method then involves splitting the time step into two equal half-steps and advancing the vorticity over each half step in turn, so that an intermediate solution, $\zeta^{k+\frac{1}{2}}_{i,j}$, at $t+\frac{1}{2}\Delta t$ is obtained. Over the first half-step, from t to $t+\frac{1}{2}\Delta t$, X-derivatives of ζ are expressed implicitly, at $t+\frac{1}{2}\Delta t$, whilst the Y-derivatives of ζ are assigned their values at time t. A solution for $\zeta^{k+\frac{1}{2}}_{i,j}$ can then be obtained as described below. Over the second half-step, from $t+\frac{1}{2}\Delta t$ to $t+\Delta t$, X-derivatives are now assigned their newly calculated values at $t+\frac{1}{2}\Delta t$, and Y-derivatives are expressed implicitly, at $t+\Delta t$. We can then obtain $\zeta^{k+1}_{i,j}$. In each of these two steps the values of $\psi_{i,j}$ and the boundary conditions are evaluated at the centres of each half time step, $t+\frac{1}{4}\Delta t$ and $t+\frac{3}{4}\Delta t$, using linear interpolation. Written in finite-difference form the above gives

$$\frac{\zeta^{k+\frac{1}{2}}_{i,j}-\zeta^k_{i,j}}{\frac{1}{2}\Delta t} = b^2AB\left[\frac{\delta}{\delta Y}\left(\zeta^k_{i,j}\frac{\delta\psi_{i,j}}{\delta X}\right)-\frac{\delta}{\delta X}\left(\zeta^{k+\frac{1}{2}}_{i,j}\frac{\delta\psi_{i,j}}{\delta Y}\right)\right] + \frac{b^2}{R}\left[A^2\frac{\delta^2\zeta^{k+\frac{1}{2}}_{i,j}}{\delta X^2}-A\frac{\delta\zeta^{k+\frac{1}{2}}_{i,j}}{\delta X}+B^2\frac{\delta^2\zeta^k_{i,j}}{\delta Y^2}-B\frac{\delta z^k_{i,j}}{\delta Y}\right], \tag{2.32a}$$

for the first half time step and, for the second half time step,

$$\frac{\zeta^{k+1}_{i,j}-\zeta^{k+\frac{1}{2}}_{i,j}}{\frac{1}{2}\Delta t} = b^2AB\left[\frac{\delta}{\delta Y}\left(\zeta^{k+1}_{i,j}\frac{\delta\psi_{i,j}}{\delta X}\right)-\frac{\delta}{\delta X}\left(\zeta^{k+\frac{1}{2}}_{i,j}\frac{\delta\psi_{i,j}}{\delta Y}\right)\right] + \frac{b^2}{R}\left[A^2\frac{\delta^2\zeta^{k+\frac{1}{2}}_{i,j}}{\delta X^2}-A\frac{\delta\zeta^{k+\frac{1}{2}}_{i,j}}{\delta X}+B^2\frac{\delta^2\zeta^{k+1}_{i,j}}{\delta Y^2}-B\frac{\delta\zeta^{k+1}_{i,j}}{\delta Y}\right] \quad (2 \leqslant i \leqslant M-1, \quad 2 \leqslant j \leqslant N-1), \tag{2.32b}$$

where $A = a-(i-1)\,\Delta X$ and $B = a-(j-1)\,\Delta Y$. Each of (2.32) results in a tridiagonal system of algebraic equations, which are solved in the usual way be forward and back substitution.

When advancing the vorticity transport equation one time step from time t through (2.32) as described above, we assume that $\psi^{k+1}_{i,j}$ and, when the no-slip boundary condition is enforced, the wall vorticity $\zeta^{k+1}_{i,1}$, $2 \leqslant i \leqslant M-1$, are known at time $t+\Delta t$. As this is, of course, not immediately true the following procedure is pursued. First estimates of $\psi^{k+1}_{i,j}$ and $\zeta^{k+1}_{i,1}$ are made from extrapolating from the two previous time steps. Using these estimates and the complete solution at time t, namely $\psi^k_{i,j}$, $\zeta^k_{i,j}$, (2.32) is solved to obtain a first estimate of $\zeta^{k+1}_{i,j}$. Solution of (2.30) and evaluation of the wall vorticity, in the manner described below, gives a revised estimate of $\psi^{k+1}_{i,j}$ and $\zeta^{k+1}_{i,1}$. These new values can then be used to again advance the solution for ζ from time t, and a better estimate of $\psi^{k+1}_{i,j}$ and $\zeta^{k+1}_{i,j}$ is thus obtained. This iteration within a time step continues until successive iterations differ by an amount which is less than a tolerance set for the calculation. For the case of the stress-free boundary condition $\zeta_{i,1} = 0$, $1 \leqslant i \leqslant M$, it is only necessary to iterate on the stream function. The above method ensures that the numerical procedure is accurate to $O(\Delta X^2, \Delta Y^2, \Delta t^2)$.

The linear elliptic equation (2.30) is solved by the successive point over-relaxation

iterative method applied to the following finite-difference form of the equation:

$$b^2\left[A^2\frac{\delta^2\psi_{i,j}}{\delta X^2}-A\frac{\delta\psi_{i,j}}{\delta X}+B^2\frac{\delta^2\psi_{i,j}}{\delta Y^2}-B\frac{\delta\psi_{i,j}}{\delta Y}\right]=-\zeta_{i,j}. \tag{2.33}$$

When a no-slip boundary condition is applied, the wall vorticity must be calculated to ensure $u = v = 0$ on $Y = 0$. This is done using Woods' (1954) second-order method, which, on being derived in the (X, Y)-plane, gives

$$\zeta_{i,1}=\frac{-6a^3b^2}{2a\Delta Y^2+3\Delta Y^3}\psi_{i,2}-\frac{a}{(2a+3\Delta Y)}\zeta_{i,2} \quad (2\leqslant i\leqslant M-1).$$

We therefore have, in the above, a procedure for numerically integrating the governing equations (2.4) and (2.5) forward in time, commencing at $t = t_I$, and ensuring that the boundary conditions are satisfied for all $t > t_I$ within the finite-difference approximation.

3. Results and discussion

To initiate a numerical integration of the governing equations (2.4) and (2.5) we must first choose the initial time t_I from which we can commence the time-marching scheme. This choice of t_I is dependent upon two factors. Firstly, the asymptotics of § 2.1 require that both t_I and t_I/R are small, for a given Reynolds number, for the expansions to be valid. Secondly, having selected the dimensions of the grid $(M \times N)$ in the transformed plane, t_I/R must be chosen such that, on setting up the initial vorticity distribution, the rotational regions are sufficiently well represented with respect to the number of grid points defining them. For all the results presented below $M = N = 51$, so that, having chosen $a = 5{\cdot}0$ in (2.28), $\Delta X = \Delta Y = 0{\cdot}1$ from (3.31). At this stage we are still at liberty to choose the parameter b in (2.28). As stated previously, b can be chosen to vary the concentration of grid points in the (x, y)-plane in regions where gradients are initially large. We must also ensure, however, that the far field is adequately represented.

For example, at $R = 50$ we have chosen $t_I = 0{\cdot}25$. This implied value of t_I/R clearly satisfies the second of the above requirements. To check the first requirement we have carried out a numerical integration for $t > t_I$ and compared the results with the asymptotic expansions. Comparison was made through the total vorticity in the flow-field defined as

$$\Gamma_T=\oint_C \mathbf{v}\,.\,d\mathbf{s}=\int_S \zeta\,dS; \tag{3.1}$$

C is a curve enclosing the region S, where S is the first quadrant $x, y \geqslant 0$. From § 2.1, (2.5) and (3.1), the asymptotic expansion for Γ_T is given by

$$\Gamma_T=1-\int_0^\infty\left\{U_0+\left(\frac{t}{R}\right)^{\frac{1}{2}}U_1+\left(\frac{t}{R}\right)\left(U_2+\frac{\partial^2 U_0}{\partial x^2}\right)\right\}dx. \tag{3.2}$$

Γ_T was calculated from the numerical results by the contour integral in (3.1), as $\mathbf{v} = 0$ on parts of C, so simplifying the calculation. Figure 1 shows the total circulation for the no-slip boundary condition for $R = 50$ from (3.2), and from a numerical integration for $t > 0{\cdot}25$ for both $b = 0{\cdot}5$ and $b = 0{\cdot}375$ to also motivate the choice of this parameter. As can be seen, the choice of $t_I = 0{\cdot}25$ was valid as the results from the numerical integrations for $t > t_I$ remain close to those obtained from the

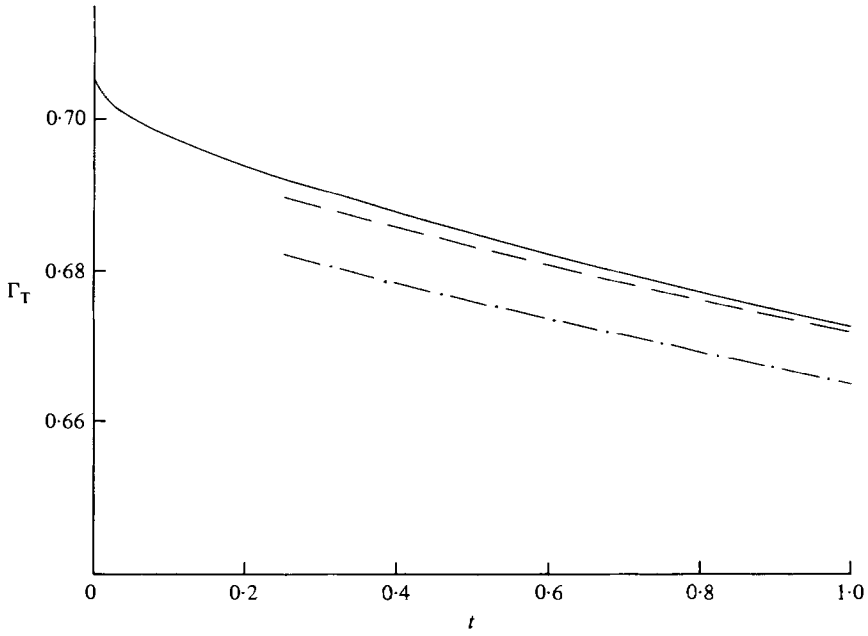

FIGURE 1. The variation of the total vorticity in the flow field for the case of a no-slip boundary with $R = 50$: ——, asymptotic result (3.2); —·—·—, numerical solution with $b = 0{\cdot}5$; — — —, numerical solution with $b = 0{\cdot}375$.

asymptotic solution. Further, the agreement is to within 1·5 % for $b = 0{\cdot}5$ but less than 0·5 % for $b = 0{\cdot}375$, for $t \leqslant 1{\cdot}0$; this latter value was chosen for all our calculations. Similar considerations for other Reynolds numbers resulted in a choice of $t_I = 0{\cdot}5$ for $R = 100$ and $t_I = 0{\cdot}75$ for $R = 150$.

Two tolerances need to be set in the numerical integration. In the iterative solution of (2.30) through (2.34), the iteration was terminated when

$$\max \left\{ \left| \frac{\psi_{i,j}^{(k+1)} - \psi_{i,j}^{(k)}}{\psi_{i,j}^{(k+1)}} \right| \right\} < 10^{-5} \quad \text{for all } i,j,$$

and in the time iteration of the stream function, and hence the vorticity, and where appropriate the wall vorticity, a solution was deemed to have been reached when a relative accuracy better than 10^{-3} was obtained between successive iterations at all grid points. These tolerances were found to give at least three-significant-figure accuracy in the results. The time step used in all the calculations was $\Delta t = 0{\cdot}05$. This value of Δt required at most five iterations per time step but mostly two were sufficient. A larger value of Δt was found to give the same results, but a larger number of time iterations were required resulting in no reduction in computing time.

Calculations for $R = 50$ were also carried out on a coarser grid with $M = N = 26$ and Richardson h^2 extrapolation was performed on the total circulation using the results from this coarse grid and the original grid. The result of this extrapolation was to give a value of Γ_T to within 0·5 % of Γ_T from the original grid, which gives further confidence in these results.

During the numerical integration two different trajectories were calculated in the (x, y)-plane for varying time. These were firstly the point of local maximum vorticity, and secondly the path of the fluid particle (X_p, Y_p) which was originally at the centre

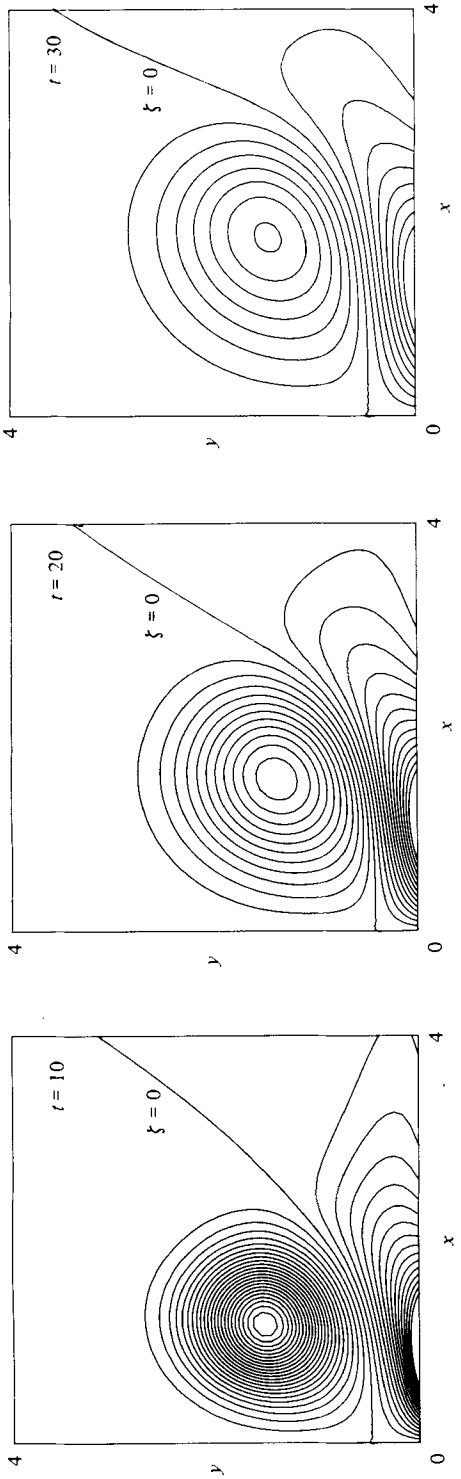

FIGURE 2. Contours of constant vorticity for the case of a no-slip boundary with $R = 100$, for various values of t. The curve $\zeta = 0$ is indicated for each value of t, with the other contours representing increments $\pm 0{\cdot}033$ in ζ for the vortex core and wall regions respectively.

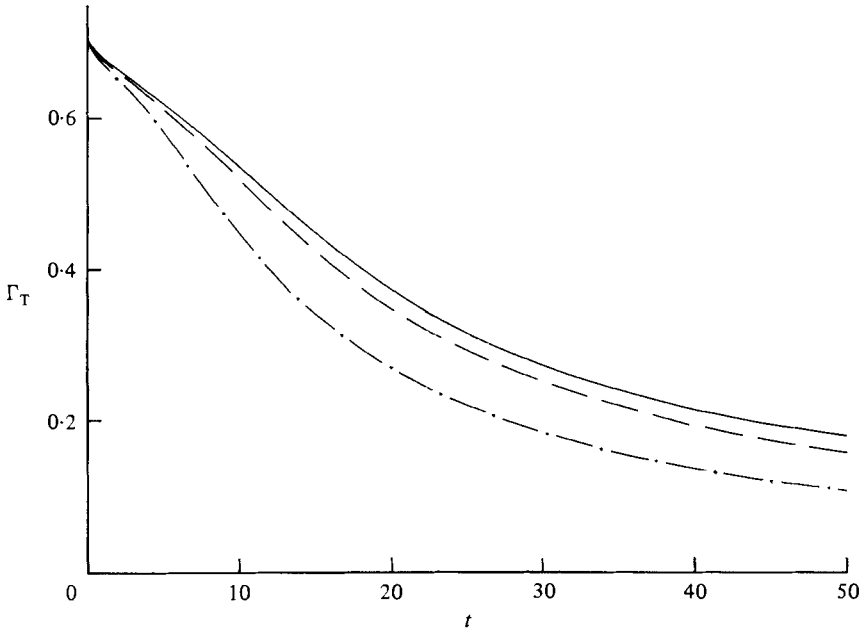

FIGURE 3. The variation of the total vorticity in the flow field for the case of a no-slip boundary for various values of R: —·—·—, $R = 50$; — — —, 100; ——, 150.

of the vortex at $t = 0$. This second trajectory is calculated by solving the equations

$$\frac{dX_p}{dt} = u(X_p, Y_p, t), \quad \frac{dY_p}{dt} = v(X_p, Y_p, t),$$

subject to $X_p(0) = x_0(0)$, $Y_p(0) = y_0(0)$.

We present results of the calculations described above, for both a no-slip boundary and a stress-free boundary, in the form of vorticity distributions across the flow-field for various values of t, the variation of the total vorticity with t, and vortex trajectories across the flow-field.

Consider first the no-slip boundary. With the initial vortex position at (1, 2), and vortex strength of unity in our dimensionless variables, there is a vortex sheet formed at the boundary within which the total vorticity is $-0{\cdot}295$. These regions of intense vorticity diffuse as t increases, and move owing to their mutual interaction. This is illustrated well in figure 2, where lines of constant vorticity are shown for various values of increasing t. We note that there is evidence of a sweeping up of negative vorticity from the wall region into the main body of the fluid, but we can report that, within the range of values of R that we have considered, flow separation from the wall does not take place. We also see, from this figure, that the total vorticity diminishes quite quickly as vorticity from the two regions diffuses; indeed the wall region may be thought of as a strong sink for the positive vorticity associated with the original vortex. This decay of total vorticity, as a function of t, is shown in figure 3 for various values of R, for which the initial asymptotic form is given by (3.2). Note that, as R increases, the total vorticity decays less rapidly, which is to be expected since diffusive effects decrease as R increases. Finally, for this no-slip case, we show in figure 4 various trajectories in the flow field. Thus we show the path traced out as t increases by the point at which the vorticity has a local maximum; this may be

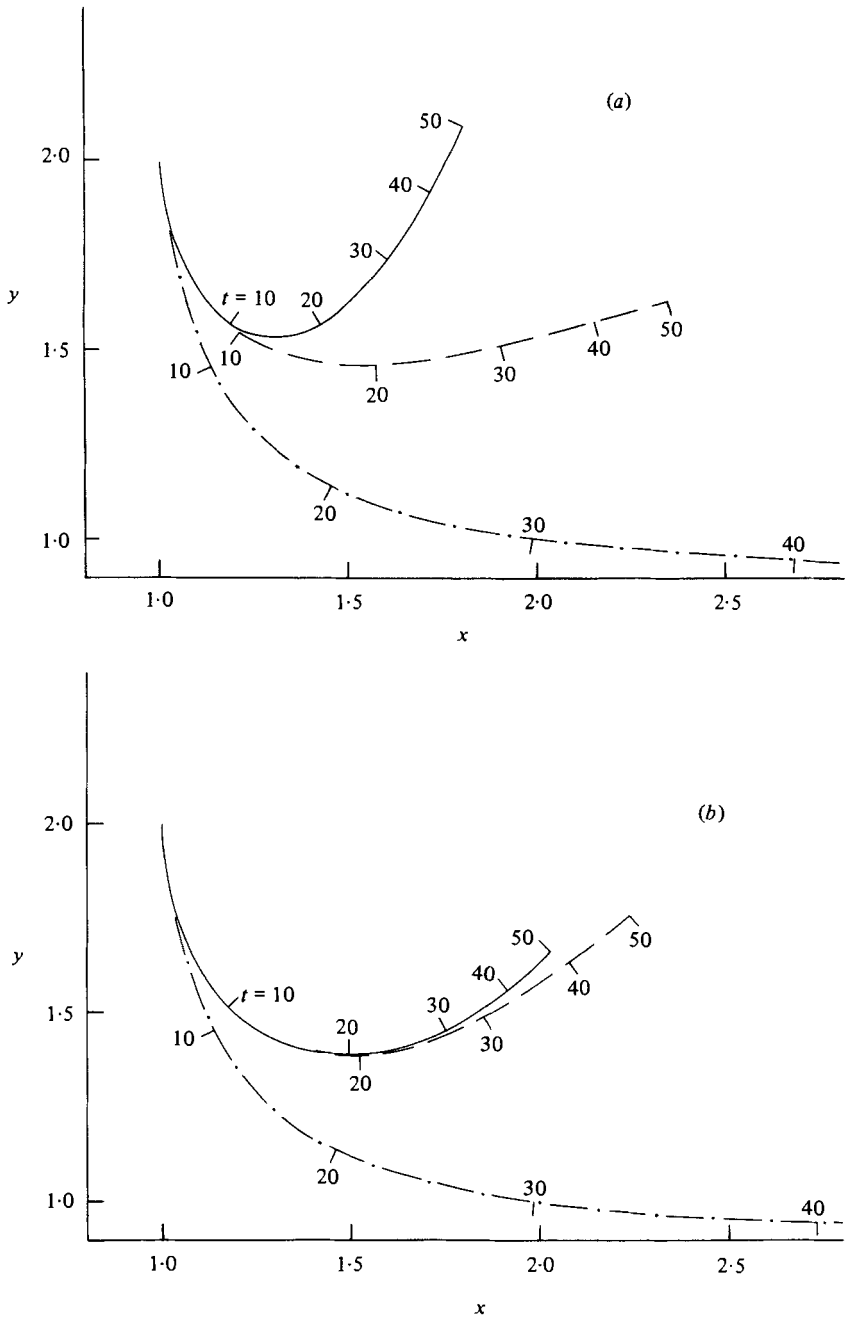

FIGURE 4. Trajectories in the flow field for the case of a no-slip boundary with (*a*) $R = 50$, (*b*) $R = 100$. ——, position of maximum vorticity; — — —, the path of the particle initially coincident with the vortex; —·—·—, the inviscid trajectory. On each trajectory positions at various values of t are indicated.

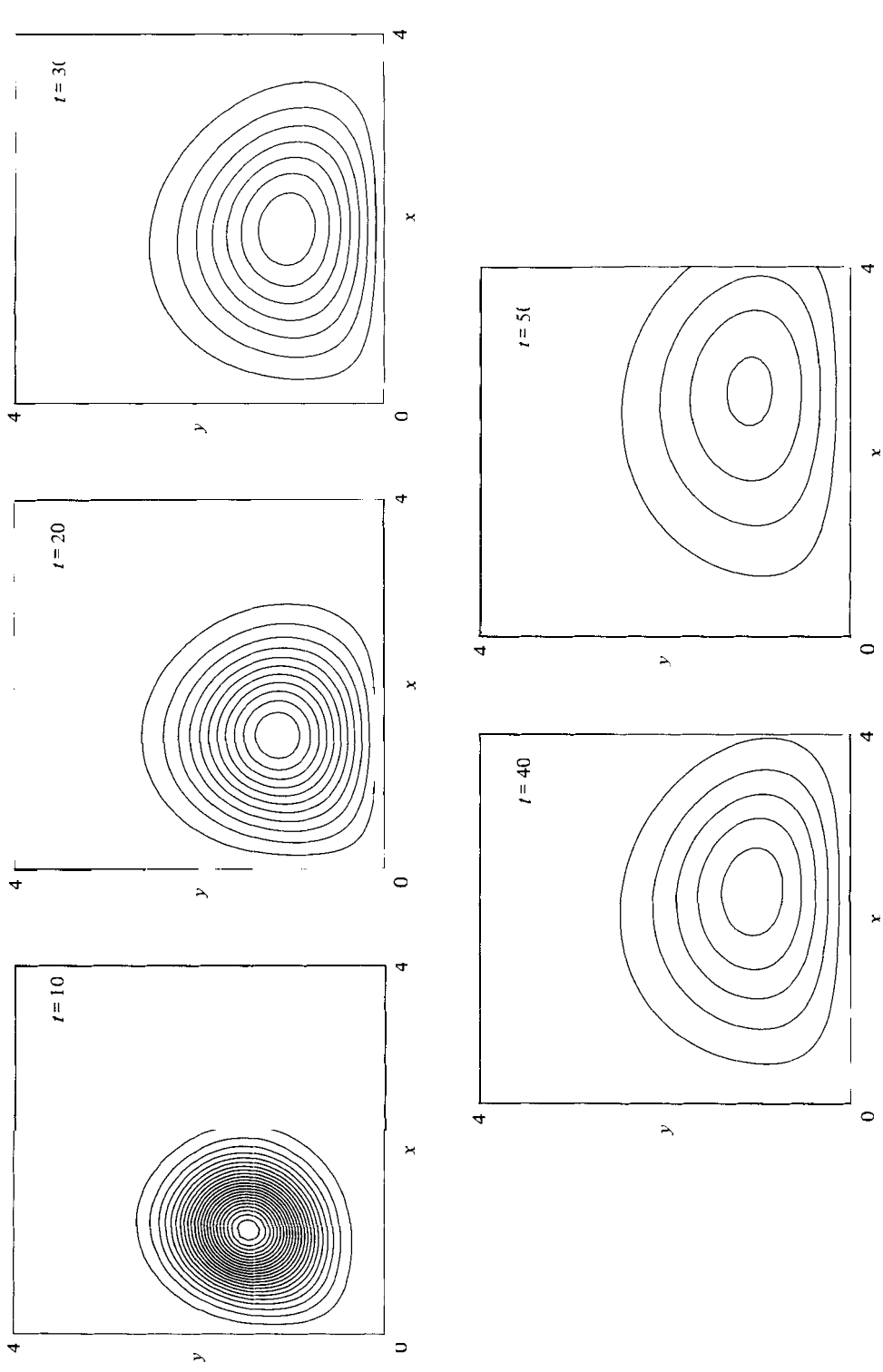

FIGURE 5. Contours of constant vorticity for the case of a zero-stress boundary with $R = 100$, for various values of t. On the lines $x = y = 0$ we have $\zeta = 0$, whilst the other curves represent increments of 0·033 in ζ.

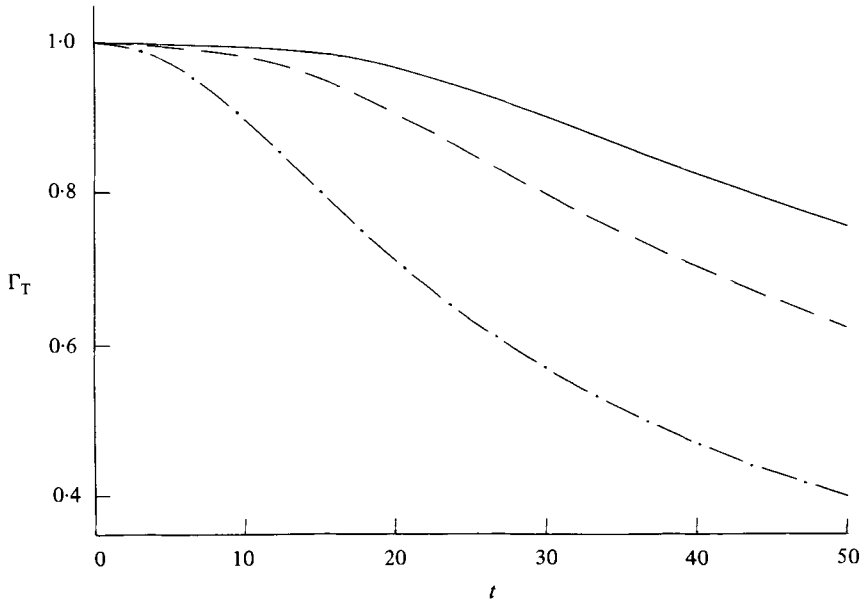

FIGURE 6. As for figure 3, but now for a zero-stress boundary.

compared with the trajectory of the line vortex, starting at (1, 2) at time $t = 0$, in an inviscid fluid, which is also shown. In addition we show the particle path for that particle of fluid which was at the point (1, 2) at the initial instant $t = 0$. In the early stages of the fluid motion these three trajectories all coincide, with that coincidence maintained for a longer period as R increases. Of particular interest is the fact that, although the vortex centre moves, in the early stages, towards the boundary, it eventually moves away, or 'rebounds', from it.

For the case of a zero-stress boundary we present the same flow characteristics in figures 5–7. The same features are present, but now in a weaker form owing to the absence of the region of intense negative vorticity at the no-slip boundary. Thus, although the boundary, at which $\zeta = 0$, still acts as a sink of vorticity, as indeed does the line of symmetry, this is relatively weak and the vorticity decays much more slowly, as may be seen in figure 5, and more explicitly in figure 6. In figure 7 we again show the three trajectories defined above and see clearly the tendency for them to coincide as R increases. This is quite marked in this case when there is only mild interference due to the presence of the boundary. We again note that the vortex centre eventually begins to move away, or rebound, from the boundary with the point x_m of minimum approach increasing as R increases. It is this phenomenon of rebounding of the vortex centre from the boundary in both the no-slip and zero-stress cases which is one of the most striking features of the results which we have obtained, and we now discuss its significance in relation to the work of others.

Papers by Dee & Nicholas (1968) and Tombach *et al.* (1975) have reported on flight-test observations of trailing vortices produced by an aircraft flying close to the ground in which the vortices after initially travelling towards the ground began to rise, or rebound, from it. Laboratory experiments designed *inter alia* to examine this phenomenon have been carried out in air by Harvey & Perry (1971), in water by Barker & Crow (1977) and in both air and water by Wickens (1980).

In the experiments of Harvey & Perry, for which $R = O(10^4)$, a vortex was shed

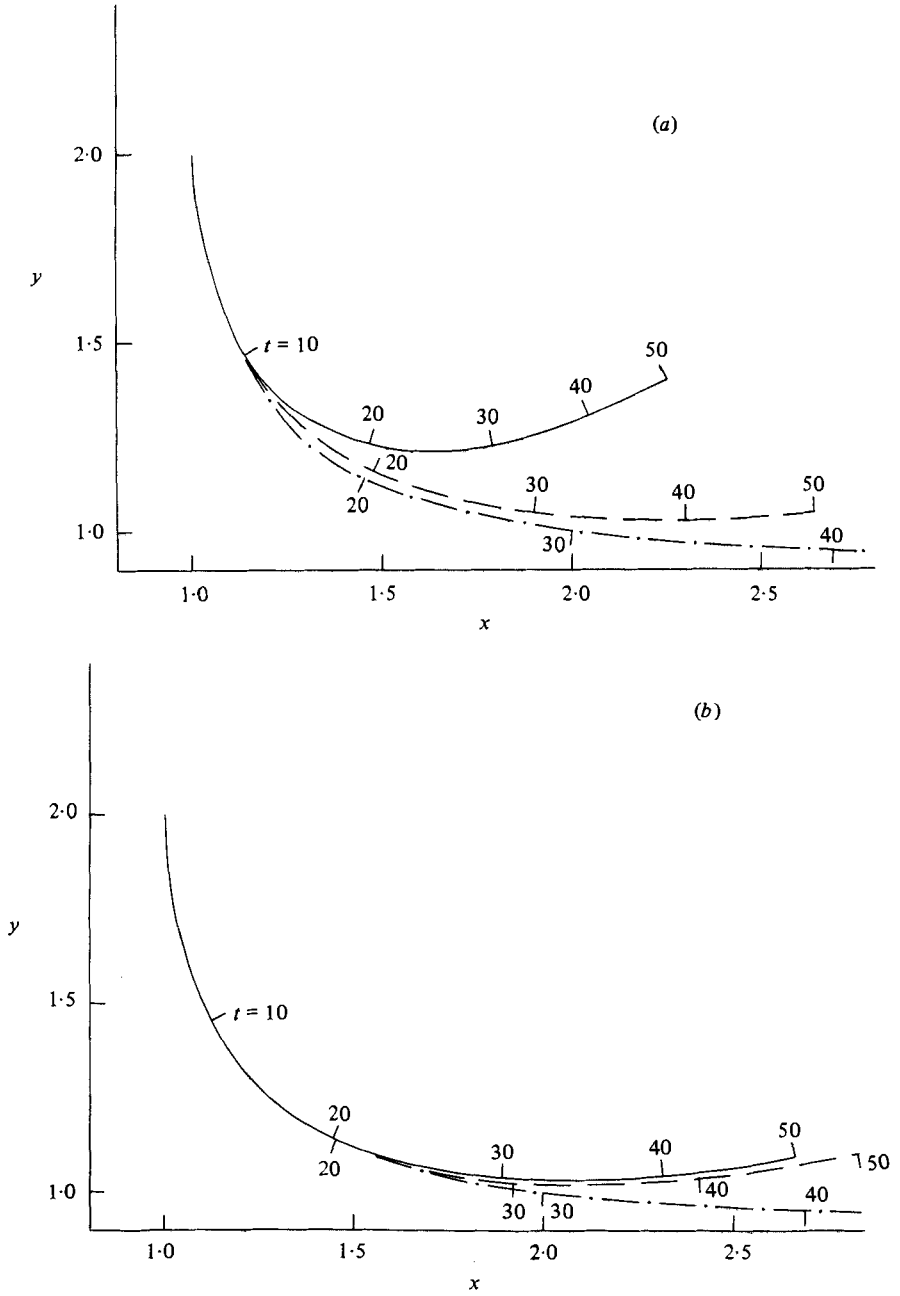

FIGURE 7. As for figure 4, but now for a zero-stress boundary.

behind a half-span wing in a wind tunnel with a moving floor. From their total-head surveys across the flow they deduce that when the vortex is sufficiently close to the tunnel floor flow separation is induced and a secondary vortex is responsible for the rebound of the main vortex. Numerical solutions of the unsteady boundary-layer equations obtained by Walker (1978), in which an inviscid line vortex translates with uniform speed parallel to a fixed boundary, and at a finite distance from it, exhibit

singular behaviour after a finite time, which is interpreted as an eruption of the flow from the boundary. This is in accord with the observations of Harvey & Perry.

The experiments of Barker & Crow were carried out in a water tank with a specially designed vortex generator from which the vortex pair was propelled vertically upwards. Again the experiments were carried out at Reynolds numbers $O(10^4)$. This configuration allowed the interaction with either a no-slip or zero-shear-stress boundary to be studied depending upon whether or not a rigid plane boundary was introduced at the otherwise free surface. The rebound phenomenon was observed not only from the rigid surface but also from the free surface for which the explanation cannot involve flow separation. Barker & Crow conjecture that the difference between observation and that which is predicted by an inviscid theory involving line vortices may be reconciled by the introduction of a finite core size into the inviscid vortex. However, Saffman (1979) shows, within the framework of inviscid theory, that it is not possible to explain the rebound phenomenon by finite core size. He observes however that since the rebound occurs for rigid or free surfaces an explanation based upon inviscid theory should be possible. We return to this point below.

The experiments of Wickens (1980) were carried out in both air and water. Few details of the experiments are given by him, and in particular it is not possible to deduce the Reynolds numbers of the flows. However, in common with the experiments described above, the vortices are seen to rebound from the rigid surface to which they were propelled.

We return now to our own results and pay particular attention to the rebound phenomenon, which is clearly demonstrated in figures 4 and 7. The first point we note is that the Reynolds numbers at which our calculations have been carried out are at least two orders of magnitude lower than those reported in the experiments. However, we believe that apart from the occurrence of flow separation, which is not a feature associated with the stress-free boundary anyway, the results for $R = O(10^2)$ exhibit most of the features observed in the experiments at higher Reynolds numbers. Consider first the case of a no-slip boundary. The occurrence of flow separation, which does not take place within our range of Reynolds numbers, as predicted theoretically by Walker (1978) and observed by Harvey & Perry (1971) must clearly have a dramatic effect upon the flow field, and will certainly induce a rebound of the incident vortex. However, even in the absence of separation the viscous displacement effect of the no-slip boundary, which is first apparent at $O\{(t/R)^{\frac{1}{2}}\}$ in the asymptotic development of § 2.1, and may be inferred from the illustrations of the flow development in figure 2, is sufficient to force the vortex away from the boundary. For the zero-stress case there is no such effect, and viscous effects are only significant at the boundary after a finite time when vorticity has diffused from the neighbourhood of the vortex to it. Thus not only are the trajectories associated with the rebounding quantitatively different in the two cases but a qualitatively different explanation from that advanced for the no-slip boundary must be sought. We believe that the explanation still involves viscous effects as follows. In the initial stages of the motion, it can be seen from figure 5 that the point of maximum vorticity, the path of the fluid particle which was originally coincident with the line vortex, and the line-vortex trajectory for an inviscid fluid are all coincident. After a finite time, which increases with increasing Reynolds number or decreasing diffusive effects, these trajectories diverge. The zero-stress boundary at which $\zeta = 0$ acts as a sink of vorticity. Thus, as vorticity diffuses up to the boundary and is lost, so the point at which the vorticity is a maximum divorces itself from the original fluid particle and now lies further away from the boundary than that particle. As this diffusive process accelerates so this

effect becomes enhanced until eventually the position of maximum vorticity is seen to move away from the boundary or rebound. There is a concomitant effect upon the fluid particle which was originally coincident with the line vortex. With the position of maximum vorticity now further away from the boundary than this particle, there is a tendency for it to be swept forward of the point of maximum vorticity under the velocity field associated with the vorticity, and ultimately, at the higher Reynolds numbers, to be swept from its more forward position to one which is also slightly further from the boundary than the point of maximum vorticity itself. All these features are apparent in figure 7, from which it is also of interest to note that in this case the three trajectories diverge simultaneously, which may be contrasted with the case of a no-slip boundary, which further emphasizes the displacement effect in that case. We can also see from figure 7 that the point at which the vortex centre is at its minimum distance from the boundary increases as the Reynolds number increases, which is what we would expect; in the experiments of Barker & Crow it is about $x = 4$. We also note, that in all cases that we have calculated, the three trajectories only begin noticeably to diverge when the total vorticity in the flow field has been reduced by about 20%. The mechanism which we have suggested as being responsible for the rebound of the vortex from a zero-shear-stress boundary will also, of course, operate in the case of a no-slip boundary, where it will reinforce the viscous displacement effect. In conclusion we re-affirm our view that the rebounding of a vortex pair from a plane boundary, even when the boundary is a free surface, is essentially a viscous phenomenon.

The authors are indebted to Mr J. H. B. Smith, RAE, Farnborough, for helpful discussion, and to SERC for financial support in the form of a studentship for A. J. P.

REFERENCES

Barker, S. J. & Crow, S. C. 1977 *J. Fluid Mech.* **82**, 659.
Bayliss, A., Gunzberger, M. & Turkel, E. 1982 *SIAM J. Appl. Math.* **42**, 430.
Blasius, H. 1908 *Z. Math. Phys.* **56**, 1.
Dee, F. S. & Nicholas, O. P. 1968 *ARC CP* 1065.
Grove, J. 1981 Ph.D. thesis, University of Manchester.
Harvey, J. K. & Perry, F. J. 1971 *A.I.A.A. J.* **9**, 1659.
Lamb, H. 1932 *Hydrodynamics*, 6th edn, p. 223. Cambridge University Press.
Roache, P. J. 1972 *Computational Fluid Dynamics*. Hermosa.
Saffman, P. G. 1979 *J. Fluid Mech.* **92**, 497.
Tombach, I. H., Crow, S. C. & Bate, E. R. 1975 *Aerovironment Inc., Final Rep. AV FR* 538.
Walker, J. D. A. 1978 *Proc. R. Soc. Lond.* A **359**, 167.
Wickens, R. H. 1980 *Can. Aero. & Space J.* **26**, 129.
Woods, L. C. 1954 *Aero. Q.* **5**, 176.